Delayed Gammas from Fast-Neutron Fission of Th^{232}, U^{233}, U^{235}, U^{238}, and Pu^{239}†

PHILIP C. FISHER* AND LEON B. ENGLE
Los Alamos Scientific Laboratory, University of California, Los Alamos, New Mexico
(Received 28 October 1963; revised manuscript received 23 January 1964)

Results of an experiment are presented in which the energy and time dependence of gammas emitted after instantaneous fast-neutron-induced fission of Th^{232}, U^{233}, U^{235}, U^{238}, and Pu^{239} were measured. Gammas having energies between 0.12 and 6.5 MeV were detected during five short time intervals between 0.2 sec and 45.0 sec after fission occurred. The measured spectra and seventeen bin distributions of the absolute number of photons/fission-sec-MeV and intercomparisons and integrations over energy and time of these distributions are given. The rate of energy emission from the products of $Th^{232}+n$ was found to be 4.5 times higher than that from $Pu^{239}+n$ during the first time interval after fission. Delayed gamma spectra from the products of $Th^{232}+n$ are noticeably harder than those from $Pu^{239}+n$ during all five time intervals measured. The several uranium isotopes' behavior is intermediate to that of the products of $Th^{232}+n$ and $Pu^{239}+n$ in both rate of energy emission and hardness of energy spectra. The significant differences in the measured characteristics of the delayed gammas from the five fissionable isotopes permit the isotopes to be arranged in a sequence. Approximate position in the sequence depends on $\bar{z}$, the average displacement of the initial fragment distribution from fission. It appears possible to predict approximate values of delayed neutron yield, which Keepin has shown to also depend on $\bar{z}$, of other fissionable isotopes on the basis of delayed gamma measurements.

I. INTRODUCTION

A STUDY has been made of the energy and time dependence of the gammas emitted after effectively instantaneous fast-neutron-induced fission of a number of nuclides. In this first of several papers on measurements of delayed gammas, the experimental method and apparatus are described and the results of spectral measurements given for the "common" isotopes Th^{232}, U^{233}, U^{235}, U^{238}, and Pu^{239}. A theoretical interpretation of some of these results has been given by Griffin.[1]

A second paper will present detailed information on the time decay of delayed gammas from 0.2 to 240 sec after fission for the "common" five isotopes. In addition, comparisons will be made of the shape of the delayed gamma spectra appearing 10 to 13 sec after fission and resulting from: (1) thermal and fast-neutron-induced fission of U^{233}, U^{235}, and Pu^{239}, and (2) fast-neutron fission of U^{234}, U^{236}, Np^{237}, and Pu^{240}. Some time-decay information and comparisons of our results with those of other workers[2–8] will also be given.

The purpose of this investigation was to obtain a quantitative description of the energy and time dependence of gammas emitted of the order of a few seconds after fission. In addition, the validity of using relative variations of these quantities to provide a criterion for ordering fissionable nuclides was to be investigated. A successful ordering procedure would allow predictions to be made for the number of delayed gammas and/or delayed neutrons emitted by a previously unexamined isotope on the basis of a simple measurement of the delayed gammas emitted by that isotope.

II. EXPERIMENTAL METHOD

A. Sample Irradiation

The experiment evolved over a period of several years and was the result of balancing a number of factors to obtain a counting rate large enough to yield a reasonable data collection time for samples irradiated in the range of fast-neutron fluxes available. A CH_2 filter was included in the experimental apparatus between the sample and the detector, to absorb fission product β's with a minimum amount of bremsstrahlung production. Irradiation of the sample was effected by Godiva II, see Fig. 1, a bare critical assembly of uranium.[9] Spectral indices[10] show that the neutron spectrum, at the sample position in the center of the assembly, is slightly softer than the Godiva I neutron leakage spectrum measured by L. Rosen of the Los Alamos Scientific Laboratory.[11]

Time distributions of leakage neutrons produced per second from two irradiations of approximately equal strength ($\frac{1}{3}\times10^{16}$ total fissions in the assembly) are given in Fig. 2. These distributions were obtained from an organic scintillator (mounted near Godiva II) which was used to generate a pulse at a fixed neutron level on

† Work performed under the auspices of the U. S. Atomic Energy Commission.
* Present address: Lockheed Missiles & Space Company, Research Laboratories, Palo Alto, California.
[1] J. J. Griffin, following paper, Phys. Rev. **134**, B817 (1964).
[2] Unpublished work of E. Fermi, L. D. P. King, F. B. Moon, and J. A. Hoffman, reviewed by K. Way and E. Wigner, Phys. Rev. **73**, 1318 (1948).
[3] J. E. Brolley, Jr., D. H. Cooper, W. S. Hall, M. S. Livingston, and L. K. Schlacks, Phys. Rev. **83**, 990 (1951).
[4] F. C. Maienschein, R. W. Peelle, W. Zobel, and T. A. Love, Proc. 2nd Intern. Conf. Peaceful Uses At. Energy, Geneva, 1958 **15**, 366 (1958).
[5] Y. I. Petrov, J. Nucl. Energy: Pt. A **12**, 129 (1960).
[6] O. I. Leipunsky, V. N. Saharov, and V. I. Tereshchenko, J. Nucl. Energy **6**, 170 (1957).
[7] J. W. Motz, Phys. Rev. **86**, 753 (1952).
[8] J. M. Wyckoff and H. W. Koch, Natl. Bur. Std., Report 4335, 1955 (unpublished).
[9] T. F. Wimett and J. D. Orndoff, Proc. 2nd Intern. Conf. Peaceful Uses At. Energy Geneva, 1959 **10**, 449 (1959).
[10] J. Grundl and A. Usner, Nuclear Sci. Eng. **8**, 598 (1960).
[11] Figure 30 of L. Cranberg, R. B. Day, L. Rosen, R. F. Taschek, and M. Walt, *Progress in Nuclear Energy* (McGraw-Hill Book Company, Inc., New York, 1956), Vol. I, Chap. 1, p. 140.

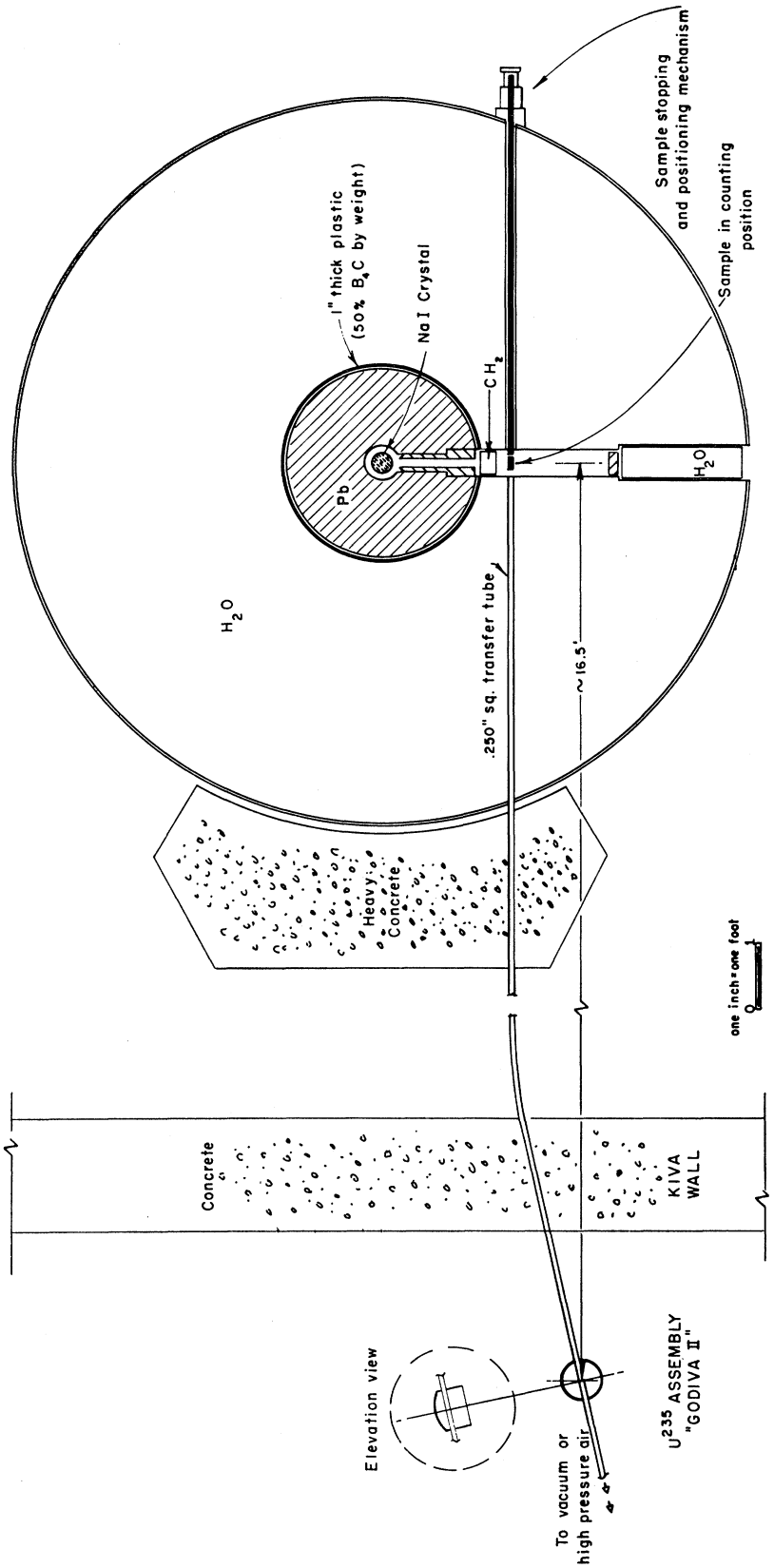

FIG. 1. Schematic of equipment used to observe delayed gamma phenomena.

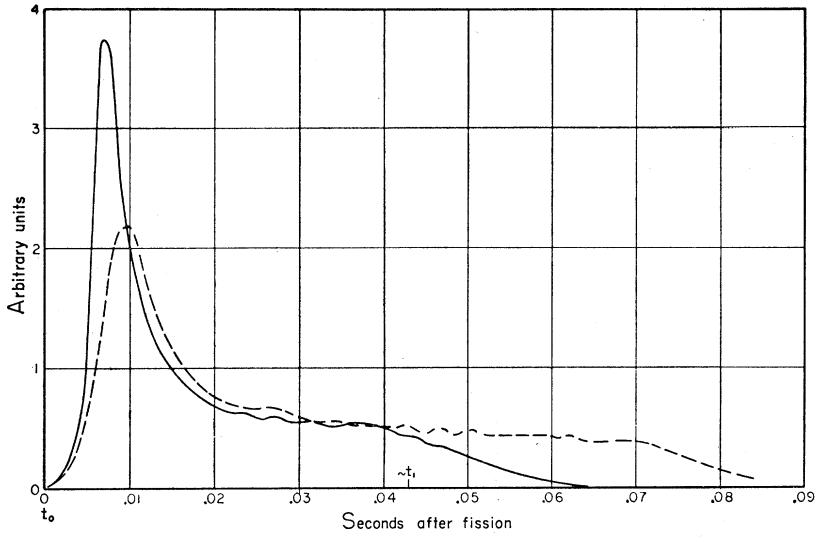

FIG. 2. Time variation of fast-neutron flux used for sample irradiation. The ordinate is proportional to the number of neutrons emitted per second.

the rising portion of the neutron burst. The time t_0 at which this level was reached was the zero of time for all experimental observations. The carrier was pneumatically ejected from the assembly slightly before the burst was completed, at a fixed time t_1 after t_0. Because of slight variation in neutron bursts, the absolute activity of a given sample varied from its average value by about $\pm 15\%$. Comparisons of Fig. 2 with the delayed gamma observation time intervals given in Fig. 12 below establishes the nearly instantaneous nature of the irradiation.

Common fissionable materials to be irradiated were made up in the form of 0.105-in. diam metal disk of different thicknesses. The composition of these fissionable materials is given in Table I. These small disks

TABLE I. Metal sample composition expressed in terms of atom percent of fissionable isotope.

Th^{232}; 100 Th^{232}
U^{233}; 96.94 U^{233}, 0.29 U^{234}, 0.04 U^{235}, <0.01 U^{236}, 2.73 U^{238}
U^{235}; 99.90 U^{235}, 0.10 U^{238}
U^{238}; 99.94 U^{238}, 0.06 U^{235}
Pu^{239}; 99.35 Pu^{239}, ~0.65 Pu^{240}, <0.02 Pu^{241}, <0.02 Pu^{242}

were placed in hardened rectangular cross-section steel carriers used with the square cross-section transfer tube. In this way, the orientation of the sample disk in the detecting geometry was fixed, and the moderately large self-absorption ($\lesssim 40\%$) of the softest gammas in the thin dimension (height) of the sample disk could be readily calculated. Small sample volumes were necessary because the transfer tube was limited to $\frac{5}{16}$-in. outside diameter. An electrical switch at the irradiation position and a phototube indicator in the stopping unit (devised by G. R. Keepin[12]) at the counting position were used to ensure that a stationary sample disk was within $\pm\frac{1}{16}$ in. for one of the appropriate positions. The time from t_0 to the beginning of the counting interval Δt and the duration of Δt were separately determined by a present electronic timer. Errors in these intervals were held to less than $\pm 1\%$.

B. Sample Counting

1. *Apparatus and Counting Conditions*

The fission-product gammas were observed with a 4-in.-diam×4-in.-long NaI total absorption spectrometer. For gamma energies less than about 2 MeV, a large total absorption crystal provides an energy resolution comparable to that obtainable from a coincidence system such as a two-crystal-Compton or a three-crystal-pair spectrometer.[13–15] Gammas which passed through the 3.1-in.-thick CH_2 absorber and the 1.072-in.-diam hole of the Pb collimator were incident on the cylindrical surface of the NaI crystal. The sample was positioned at 19.5 in. from the crystal end of the 12.75-in.-long Pb collimator. A thorough description of the crystal's response to various energy gammas is given in the Appendix. A Dumont 6364 photomultiplier and a Los Alamos model 250-A amplifier system were used to process the crystal signal.

After amplification, pulses were height analyzed by a time-gated 100-channel analyzer, and simultaneously passed through a unit-gain line-driving amplifier into a pair of single-channel analyzers. Excess pulses, those above the channel window, from each of the single-channel analyzers were made uniform in pulse height and then fed into two recording time delay analyzers.[16] Each irradiated sample produced two kinds of data: (1) a pulse-height distribution for a large energy interval for a given time interval after fission, and (2) continuous

[12] G. R. Keepin, T. F. Wimett, and R. K. Zeigler, J. Nuclear Energy **6**, 1 (1957).

[13] T. H. Braid, Phys. Rev. **102**, 1109 (1956).

[14] H. I. West, Phys. Rev. **101**, 915 (1956).

[15] C. C. Trail and S. Raboy, Rev. Sci. Instr. **30**, 425 (1959).

[16] P. G. Koontz, C. W. Johnstone, G. R. Keepin, and J. D. Gallagher, Rev. Sci. Instr. **26**, 546 (1955).

records of counting rate for times between ~0.2 sec and ~300 sec after fission for all pulses greater than the two different fixed pulse heights. By subtracting the information recorded by the two time delay analyzers, the counting rate for the pulse height equivalent to a given energy interval could be obtained.

Protection of the large NaI crystal from the gammas and neutrons produced by Godiva II required a massive shield. A calculation using removal cross sections for fission spectrum neutrons[17] gave the approximate thickness of H_2O required to reduce the counting rate expected from Godiva II burst generated delayed neutrons to an acceptable level. Supplementary calculations established the amount and distribution of Pb shielding required to protect the crystal from the gammas from fission in Godiva II and from the 2.2-MeV hydrogen capture gammas arising in the neutron removal process. The building housing the Godiva II source had one foot thick concrete walls. By placing the shielded tank outside the building, the source, as well as the detector, became shielded and the burst caused background was kept to a workable level.

The characteristics of each irradiation were governed by the particular 100-channel information sought. Pulse-height distributions were taken at two different instrument sensitivities, 100 V = 100 channels = 2 MeV with the bias at 0.12 MeV, and 100 V = 100 channels = 5 MeV with the bias at 1.5 MeV. These are labeled the 2- and 5-MeV scales, respectively. The set of time channels used was 10–10 sec intervals taken to give the NaI crystal background and carrier activity preceding each burst; then, starting at t_0: 10–0.010 sec; 29–0.10 sec; 27–1.0 sec; and 32–10.0 sec intervals. To obtain pulse-height distribution data as quickly as possible, counting rates into the 100-channel analyzer averaged ~7000 counts/sec and not infrequently reached 12 000 counts/sec.

The difference between the background preceding a burst and that which occurred during the period of gamma observations was due principally to the $Fe^{56}(n,p)Mn^{56}$ reaction in the 1.8-g sample carrier. By keeping a large time interval between irradiations of a given sample and its associated Fe carrier, the residual activity of the combination was kept negligible.

A measure of the quality of the spectrum from a given irradiation was obtained by finding the probability of a count lying in channel 5 through 9 or in channel 65 through 69. Departure of either of these probabilities from its appropriate average value (for all runs) by more than three standard deviations was taken as sufficient cause to discard a run. Only the results of six irradiations were so rejected.

2. *Recording System Accuracy*

Because of the high counting rates employed, the rapid variation in time of these counting rates, and the known photomultiplier fatigue effects,[18–20] the general behavior of the counting system was rather thoroughly investigated. Amplifier gain was checked every two to three irradiations (every several hours) with radioactive sources of Zn^{65} and Na^{24} for the 2- and 5-MeV scales, respectively. The gain on each scale as measured in this manner was kept constant within a standard deviation of $\pm 1.4\%$ for all of the data taking runs.

To determine whether gain or bias shifts occurred, measurements were made with several different intensity radioactive sources: Cs^{137} (2 counts/sec), Zn^{65} (900 counts/sec), Na^{24} (1 to 15×10^3 counts/sec), and In^{116} (0.5×10^3 to 1×10^5 counts/sec). Following the count in the 1.274-MeV In^{116} photopeak over three to four half-lives always yielded a half-life within $\pm 1\%$ of the accepted 54.0-min value. On the basis of the In^{116} results, less than $\frac{1}{2}\%$ gain and $\frac{1}{2}$-V bias shift occurred for counting rates and photomultiplier anode currents three times higher than permitted for the 2-MeV scale data. Mostly because of the very low counting rates at the higher photon energies, a less conservative approach was taken in obtaining 5-MeV scale data. Most all of these data were taken at anode currents which correspond to In^{116} counting rates less than 6×10^4 counts/sec. Less than a one percent gain and less than a two-volt bias shift had been measured at these rates.

Tests were also made with highly active In^{116} samples exposed momentarily to the NaI crystal to see if the transient nature of the delayed gamma signal had any influence on the gain or base line of the system. Measurements for the gains and the recording time intervals used in the experiment showed no gain shift or base line jitter within the measuring error of ~2% (caused by poor statistics), at least up to the 6×10^4 counts/sec In^{116} rate. Although In^{116} does not decay nearly as rapidly as a fission sample and does not produce a fission gamma-like spectrum, the measurements indicate that any fatigue effects from high counting rates, during the counting intervals used, must have been quite small.

Required corrections for low-channel distortion effects were numerically evaluated by measurements of the spectrum shape at different counting rates for a given time interval after fission. The distortion was due to gate pulse effects resulting from the analyzer's self-gated mode of operation. The bias appropriate to the analyzer input-derived gate pulse had to be fixed as well as the bias appropriate to the pulse to be analyzed. Because the analyzer tended to store the largest pulse present during a given gate pulse, effectively improper sampling of spectra occurred for the first dozen or so channels for the very high input counting rates. Corrections for this amounted to roughly 25% in the first channel, and were less than $\frac{1}{2}\%$ at channel twelve and above and so could be neglected in the higher energy channels.

Since the 100-channel part of the system was normally

[17] T. Rockwell, III, Editor, Reactor Shielding Design Manual No. T10-7004, p. 52, 1956 (unpublished).

[18] P. R. Bell and R. C. Davis, Rev. Sci. Instr. **26**, 726L (1955).
[19] L. Cathey, IRE Trans. Nucl. Sci. **5**, 109 (1958).
[20] R. Hiebert (private communication).

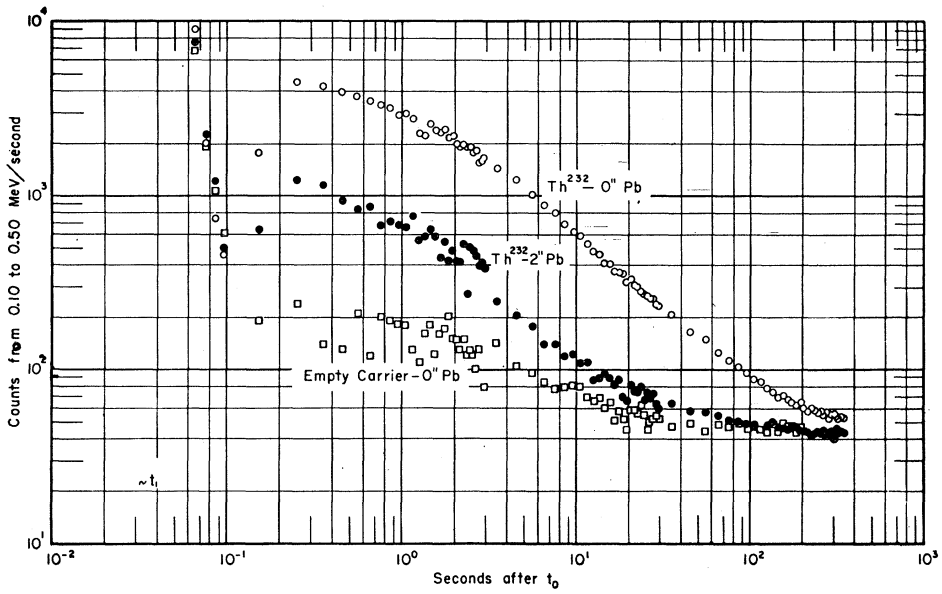

FIG. 3. Delayed gamma decay information obtained for evaluating delayed neutron effects from Th^{232}.

used to obtain spectrum shape only, losses due to high counting rates were unimportant so long as they did not distort the spectrum. For the counting rate normalization measurements, rates were held down so that a blocking time correction of only a few percent was needed. Since any spectrum distortion in the amplifier should be expected to influence the time delay analyzer records, only those irradiations which produced the lowest counting rates were used to derive the time decay data.

C. Delayed Neutron Effects

Th^{232}, which emits the largest number of delayed neutrons per fission, was chosen to determine if a large portion of the crystal counting rate was attributable to delayed neutrons emitted by the sample. Since neutron effects appear primarily in the form of low-energy inelastic or capture gamma peaks, measurements were made on the 2-MeV scale for the 1–2 sec time interval after fission. The results are given in Figs. 3 and 5. In Fig. 3 the initial rise and fall in counting rate is attributed to burst caused background; the later rise in counting rate indicates the sample has arrived at the counting position. Pulse-height distributions for an empty and a Th^{232}-loaded carrier were observed with and without a 2-in.-thick Pb shutter swung into position between the sample and CH_2 absorber. While pulses from gammas from the irradiated Th^{232} sample which succeeded in penetrating the Pb were observed, these measurements indicate only a small, $\lesssim 5\%$, portion of the crystal count rate could be due to delayed neutrons emitted from the sample.

D. Counting Rate Normalization

Part of the data necessary for the absolute normalization of pulse-height distributions was obtained from radiochemical determinations of the number of fissions produced in samples whose fission fragment gammas has been detected by the NaI crystal. The latter measurements were made on the 2-MeV scale with low-self-absorption samples which were counted for 10 to 13 sec after fission. Only counts appearing in the 1.5–2.0 MeV (pulse-height equivalent) interval were used. $4\pi\beta$ counting of the Mo^{99} product combined with an accurately known value of the probability of obtaining one Mo^{99} atom/fission lead to the number of fissions produced in the sample. The estimated error in this number of fissions was around $\pm 5\%$. Table II gives the basis of the absolute normalization obtained for the different isotopes which were extensively measured during the experiment. The larger error of the Pu^{239} result is attributed to difficulties with the chemistry involved. A less severe but still noticeable difficulty with Pu chemistry seems to have occurred for the delayed neutron investigations carried out at this laboratory.[21]

TABLE II. Radiochemical basis of normalization constants from analysis of the number of fissions produced in selected samples. The absolute number of counts in the 1.5- to 2.0-MeV pulse-height equivalent interval were obtained for the 10 to 13 sec time interval after fission.

Isotope	232	233	235	238	239
Number of samples averaged	3	3	3	3	4
Error (%)	5.0	3.6	6.2	4.3	20

A second piece of information necessary for the normalization procedure used was the time variation of the counting rate of pulses in the 1.5–2.0 MeV (pulse-height equivalent) interval. Validity of this information was checked by measurements at several different

[21] G. R. Keepin (private communication).

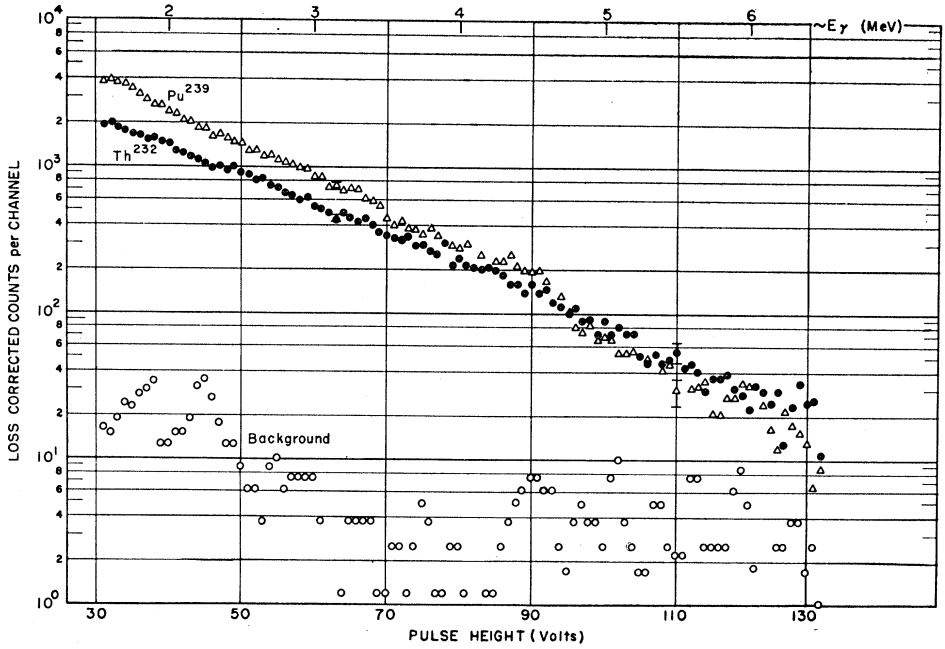

FIG. 4. Typical blocking time corrected pulse-height distributions obtained on 5-MeV scale. The Pu^{239} and background data represent 15 irradiations each, while the Th^{232} data represents only 14 irradiations. All data was taken for $\Delta t = 1$–2 seconds after t_0.

counting levels of the shape of the curve of counting rate versus time after fission. Within about two percent, no rate dependence could be found. Measurements with In indicated less than a few percent gain and/or less than a few volt bias shift could have occurred for this data. The time decay normalization constants and the instant of time at which the counting rate over each time interval had its average value were found to be accurate to $\pm 3.5\%$. The single exception to this rule is the constants for the arbitrarily selected base time interval of 10–13 sec, where a $\pm 2.5\%$ error applies.

III. DETERMINATION OF PHOTON SPECTRA

A. Pulse-Height Data Assembly

A number of operations had to be performed on the measured pulse-height distributions in order to obtain a distribution from which a photon spectrum could be derived. Each run contributing to a given spectrum was corrected successively for analyzer blocking time and low-channel distortion. All so corrected runs for a given isotope, energy, and time, were then added together and the proper background subtracted. Because of the relatively few counts per channel, the results of this assembly procedure are not too accurate in the high-energy portion of a spectrum. The data points of Figs. 4 and 5 indicate that crude background corrections would have been sufficient for photon energies up to about 5.0 MeV.

An absolute number of counts emitted in the 1.5 to 2.0 MeV (pulse-height equivalent) interval per second per fission was obtained for each counting time interval and isotope by combining the time analyzer and radiochemical normalization data. Ratios were then formed by dividing these absolute numbers by the sum of the counts in the 1.5 to 2.0 MeV (pulse-height equivalent) interval of the related set of loss, distortion, and background corrected 100-channel data. Multiplication of each number in the 100-channel set by the ratio appropriate to the set effected the conversion to counts/sec-MeV-fission. The 5-MeV scale data were fitted to the 2-MeV scale measurements by requiring identity of counting rate in the 1.7 to 2.1 MeV (pulse-height equivalent) interval.

Next, the 200 overlapping data channels, which constituted a given spectrum were reduced to 17 contiguous bins by adding together the data from neighboring channels. This reduction of resolution was performed in order to simplify the transformation of pulse-height distributions into photon spectra. Taking the full width at half-maximum of a full energy peak to be 2.3σ, the bin widths are approximately 4σ wide.

B. Photon Calculation Procedure

A photon spectrum $\gamma(k)$ emitted by the fission fragments can result in a pulse-height distribution $P(\epsilon)$ being observed by the crystal spectrometer, where k refers to the photon energy and ϵ to the pulse height. These two distributions are related by the equation

$$P(\epsilon)=\int_0^{k_{\max}} \gamma(k)R(k,\epsilon)dk, \qquad (1)$$

where $R(k,\epsilon)$ is labeled the response function of the spectrometer and $k_{\max}$ is the maximum energy of $\gamma(k)$. The response of the crystal to an effectively infinite number of monochromatic photons of energy k is a particularly shaped distribution of pulse heights ϵ.

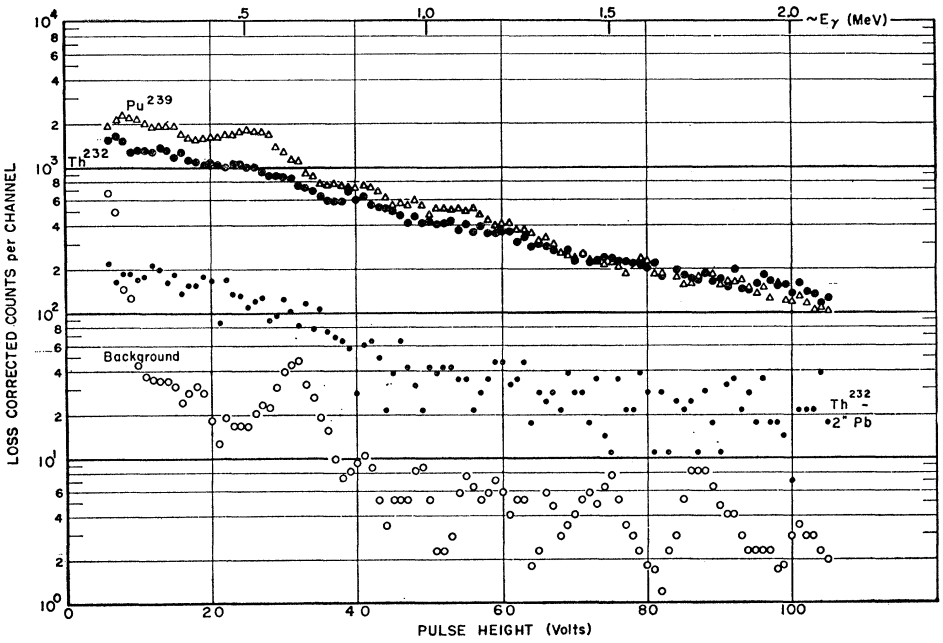

FIG. 5. Typical blocking time corrected pulse-height distribution obtained on 2-MeV scale. Each set of points represents seven irradiations taken for $\Delta t=1$–2 sec after t_0. The 2-in. Pb data for Th^{232} represents only two irradiations, having been normalized to seven irradiations so as to be directly comparable to the other data.

Integration over a small pulse-height interval $\Delta\epsilon$ allows Eq. (1) to be readily transformed to the matrix equation

$$P=\gamma R, \tag{2}$$

where P and γ are one row matrices and R is a triangular matrix. The elements in each row of R correspond to the probability for detection of a source emitted photon of energy k. That is, each row represents the pulse-height distribution for a given photon energy; the area of the distribution representing the absolute detection efficiency for that same photon energy. A mathematically unique solution to Eq. (2) exists only if R is nonsingular.

A number of workers have presented detailed descriptions of solutions of Eq. (1) found for experiments on gammas over a range of energies.[22–30] In the present case, the expression was multiplied by the inverse R^{-1} to obtain

$$PR^{-1}=\gamma. \tag{3}$$

Division of each of the elements of γ by the associated bin width $\Delta\epsilon$ and the correction of each element for sample self-absorption, yielded the final results which are presented in the next section.

The response function of $R(k,\epsilon)$ was constructed from the information contained in Figs. 15 through 17. The distribution curve for a given k (the photon energy at the center of one of the seventeen energy bins) was obtained by interpolating between the measured crystal responses given in Figs. 16 and 17. The area under the distribution curve for each k was normalized to unity; the fraction of the area located in each pulse-height interval, or bin, was determined, and each of these fractions was then multiplied by the total crystal efficiency for that k. The set of numbers which were obtained for the different values of k comprise the triangular matrix R, a portion of which is given in Table III. An extra low-energy 0th bin was used in all pulse-height distributions and in the crystal response function and its inverse in hopes of obtaining a more accurate value for the lowest real photon energy bin. While Tables III and IV list the matrix elements for the 0th interval, the final results which are presented in the next section are given for intervals one through seventeen only.

R^{-1}, the inverse triangular matrix was obtained with the aid of a 704 computer and is given in Table IV. The product of matrices R and R^{-1} is nearly a unitary matrix as all diagonal elements in the product are equal to one within the precision of the computing method and all off diagonal elements are zero or less than 10^{-8}.

Several off-diagonal elements of R^{-1} are positive and therefore indicate errors which exist in the crystal response function. The combination of the rather coarse mesh of R^{-1}, and the relatively smooth pulse-height distributions appears to result in the computed fission spectra being fairly insensitive to this type of error. At least no particularly noticeable oscillations occur in the

[22] J. W. Motz, Phys. Rev. **100**, 1560 (1955).
[23] N. Starfelt and H. W. Koch, Phys. Rev. **102**, 1598 (1956).
[24] E. A. Edelsack, W. E. Kreger, W. Mallet, and N. E. Scofield, USNRDL-TR-237, 1958 (unpublished).
[25] J. H. Hubbell and N. E. Scofield, IRE Trans. Nucl. Sci. **5**, 156 (1958).
[26] H. W. Koch and J. M. Wyckoff, IRE Trans. Nucl. Sci. **5**, 127 (1958).
[27] H. M. Childers, Rev. Sci. Instr. **30**, 810 (1959).
[28] J. Kockim and N. Starfelt, Nucl. Instr. Methods **4**, 171 (1959).
[29] W. R. Burrus, IRE Trans. Nucl. Sci. **7**, 102 (1960).
[30] N. E. Scofield, USNRDL-TR-447, 1960 (unpublished).

TABLE III. Elements of response function matrix R_{ij} for 4th, 8th, and 12th rows. The listed photon energy k applies to the midpoint of the energy bin represented by the ith row, while the pulse height ϵ applies to the center of the pulse-height interval represented by the jth column. Actual matrix elements are 10^4 times smaller than the values listed.

$j=$	0	1	2	3	4	5	6	7	8	9	10	11	12	13
$i=4$ $k=0.502$ MeV	0.037	0.068	0.104	0.125	0.666	0	0	0	0	0	0	0	0	0
$i=8$ $k=1.337$ MeV	0.025	0.043	0.057	0.070	0.089	0.106	0.153	0.158	0.564	0	0	0	0	0
$i=12$ $k=2.865$ MeV	0.016	0.020	0.024	0.032	0.037	0.045	0.053	0.062	0.073	0.107	0.181	0.302	0.487	0

TABLE IV. Inverse response function R_{ij}^{-1} using Table III notation. Actual matrix elements are ten times larger than values listed.

i/j	0	1	2	3	4	5	6	7	8	9	10	11	12	13	14	15	16	17
0	3226																	
1	−340	2193																
2	−168	−290	1786															
3	−120	−190	−306	1515														
4	−96	−143	−222	−284	1502													
5	−91	−104	−144	−251	−260	1563												
6	−58	−73	−107	−127	−311	−307	1664											
7	−28	−39	−42	−47	−171	−393	−407	1773										
8	−29	−42	−40	−48	−56	−100	−337	−497	1773									
9	−33	−26	−27	−35	−35	−59	−105	−302	−580	1808								
10	−19	−18	−8	−17	−14	−28	−58	−88	−225	−740	1876							
11	−19	−7	−9	−5	−15	−26	−32	−41	−61	−189	−962	1988						
12	−19	−7	−1	−11	−4	−6	−14	−27	−6	−5	−101	−1232	2053					
13	−7	−2	−8	−0	−6	−8	−15	−35	−71	−61	72	161	−1456	2062				
14	−1	−5	−2	−6	−7	−6	−11	−15	−10	−35	−117	−51	426	−1632	2083			
15	−3	6	2	5	−2	−5	−8	−16	−25	−23	−8	−86	−215	652	−1762	2114		
16	4	−6	−0	−3	−7	−2	−3	−5	−11	−14	−31	−12	1	−384	816	−1862	2128	
17	−2	10	2	1	−4	0	−4	−12	−11	−11	−12	−36	−65	137	−551	1011	−1952	2114

high-energy portion of the computed spectra where such errors normally exert their greatest influence.

IV. COMMON ISOTOPE RESULTS

A. Differential Spectra

Logarithmic plots of results for the various isotopes are given in Figs. 6 through 10. Each set of data is for a given time interval after fission, successively lower photon emission rates appearing at successively later times. Parts (a) and (b) of each figure correspond respectively to the original 100-channel pulse-height distributions and to the final 17-bin photon distributions. Because of poor analyzer response, the first channel of data at each energy resolution was not used in obtaining the photon spectra. The dashed vertical line at the pulse-height equivalent of 5.5 MeV is drawn in to indicate the general region where appreciable amplifier pileup effects may exist. Table V provides some pertinent information about the experimental conditions associated with the pulse-height data and their derived photon distributions.

TABLE V. Some characteristics of the experiment.

Isotope	t_{av} for time interval	2-MeV scale: Sample thickness in mg/cm²	2-MeV scale: Number of irradiations	5-MeV scale: Sample thickness in mg/cm²	5-MeV scale: Number of irradiations	% pileup in bin 14
Th^{232}	0.345	650	11	1440	11	5
	1.46	650	7	1440	14	3
	4.72	650	10	1440	14	1
	11.35	650	6	1440	10	1
	39.8	650	5	1440	9	1
U^{233}	0.345	95	12	305	13	9
	1.46	95	11	270	12	11
	4.72	230	6	540	10	7
	11.35	240	4	540	4	12
	39.8	240	2	540	4	3
U^{235}	0.345	57	11	200	13	20
	1.46	57	7	310	8	11
	4.72	110	6	510	8	9
	11.35	200	4	510	3	11
	39.8	200	2	510	5	2
U^{238}	0.345	190	9	530	10	14
	1.46	190	6	1140	7	13
	4.72	330	7	2460	6	12
	11.35	330	4	2460	3	13
	39.8	330	4	2460	5	3
Pu^{239}	0.345	74	10	170	16	15
	1.46	74	6	270	14	10
	4.72	170	6	530	10	12
	11.35	270	4	530	4	14
	39.8	270	3	530	6	3

Figure 11(a) gives the ratios of the 17-bin photon distributions of U^{235} data, normalized to unity during the first time interval after fission. Figures 11(b) and (c) present the relative shapes of the photon spectra as inferred from the 17-bin photon distributions for each of the different isotopes for the earliest and latest time intervals after fission. To normalize Fig. 11(b) and (c) data, the photon distribution of U^{235} for each time interval was arbitrarily set equal to unity.

B. Errors in Differential Spectra

The experimental sources of error in the photon spectra may be conveniently separated into three categories: (A) statistical errors affecting both the shape and absolute magnitude of the spectra, (B) statistical errors which influence only the absolute magnitude of a given spectrum, and (C) systematic errors caused by amplifier pulse pileup effects. Where relative spectral hardness is the only item of concern, (B) errors may be

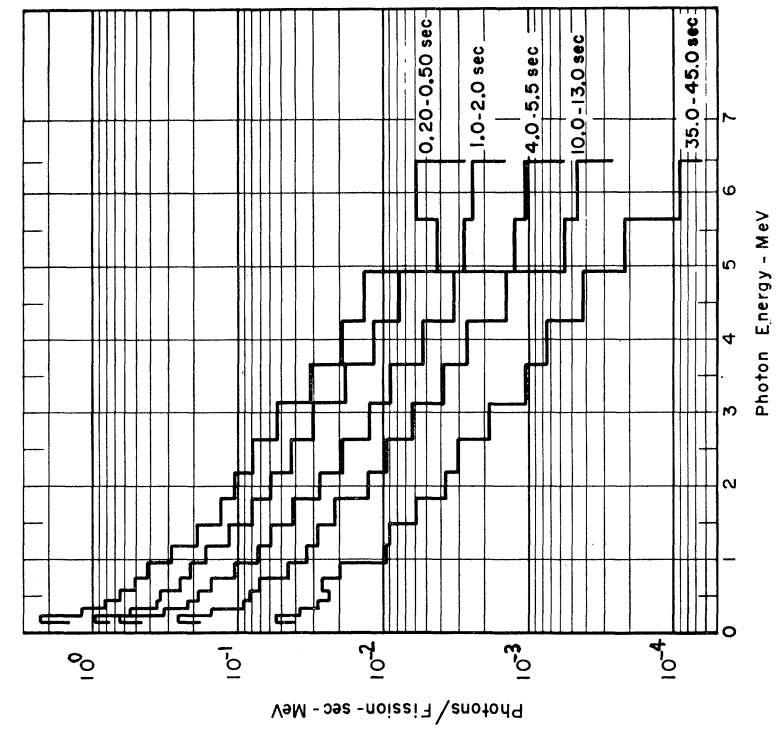

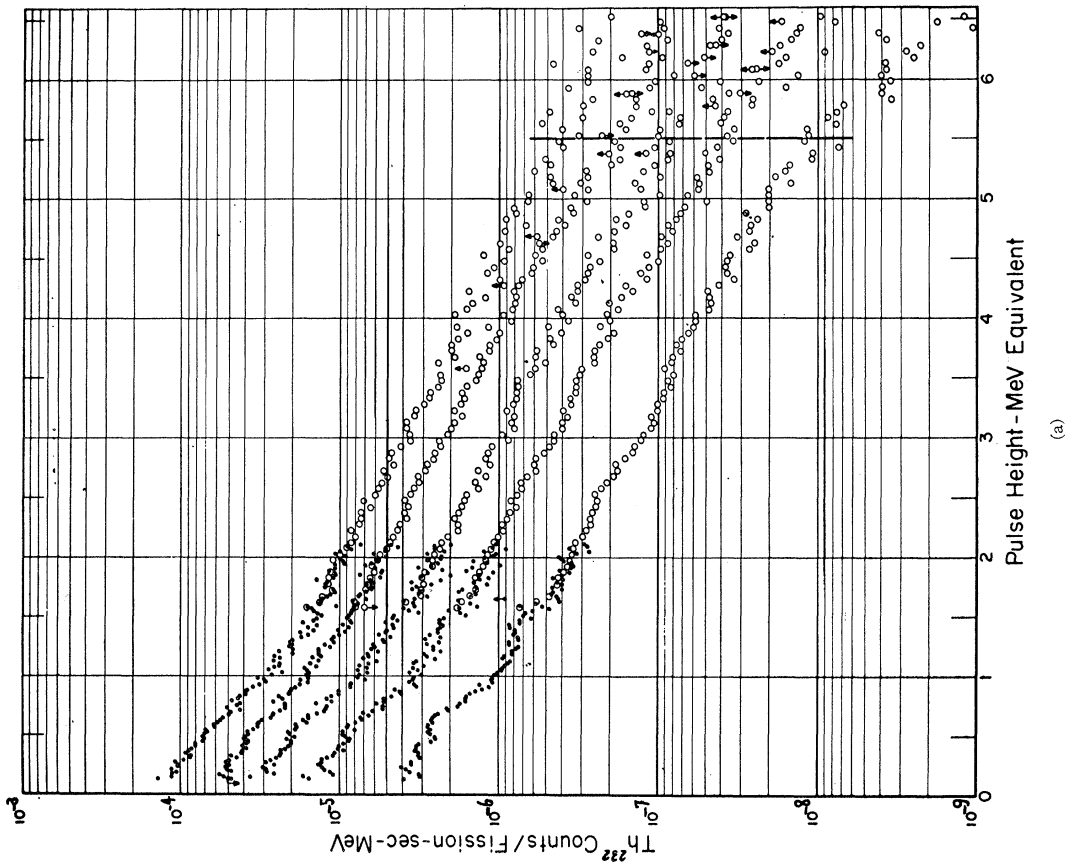

FIG. 6. Results of Th^{233} differential photon spectra versus energy for different time intervals after fission expressed as (a) normalized 100-channel pulse-height distributions, and (b) fully corrected 17-bin photon distributions.

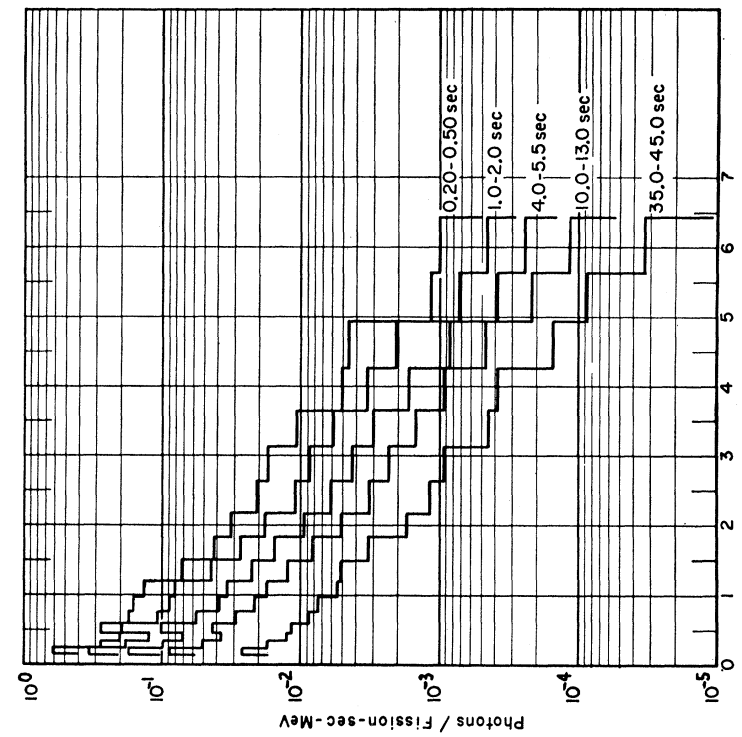

(b)

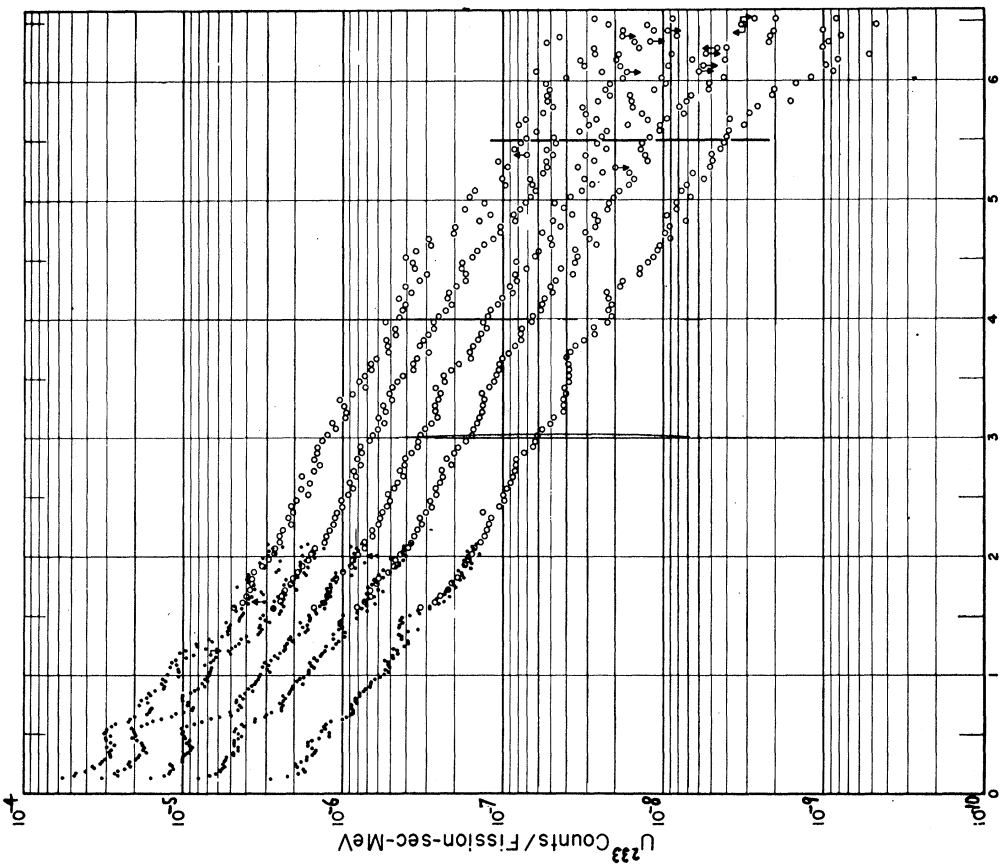

(a)

FIG. 7. Results of U^{233} differential photon spectra versus energy for different time intervals after fission expressed as (a) normalized 100-channel pulse-height distributions, and (b) fully corrected 17-bin photon distributions.

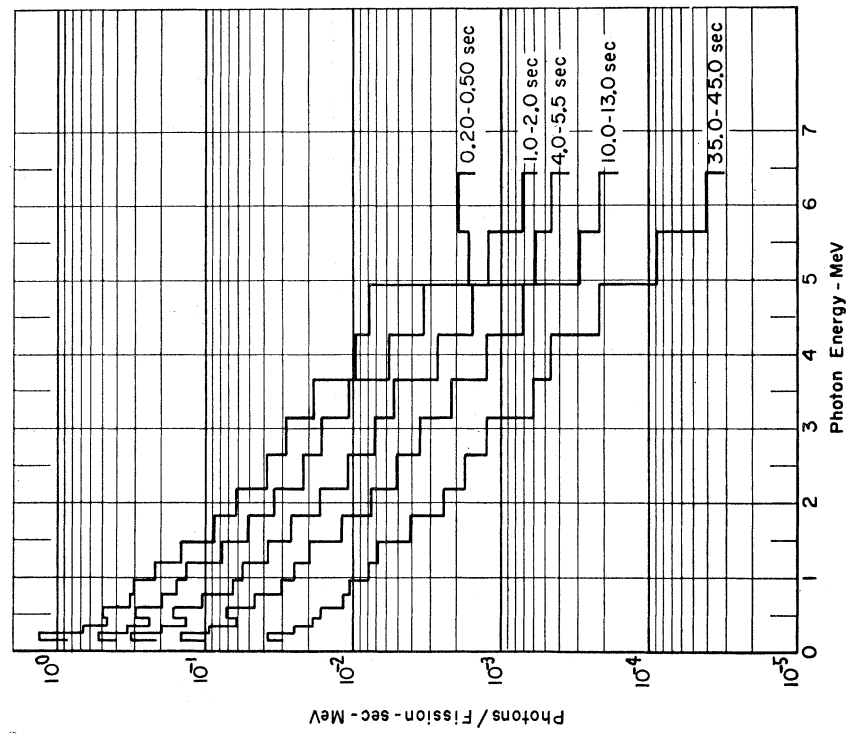

(b)

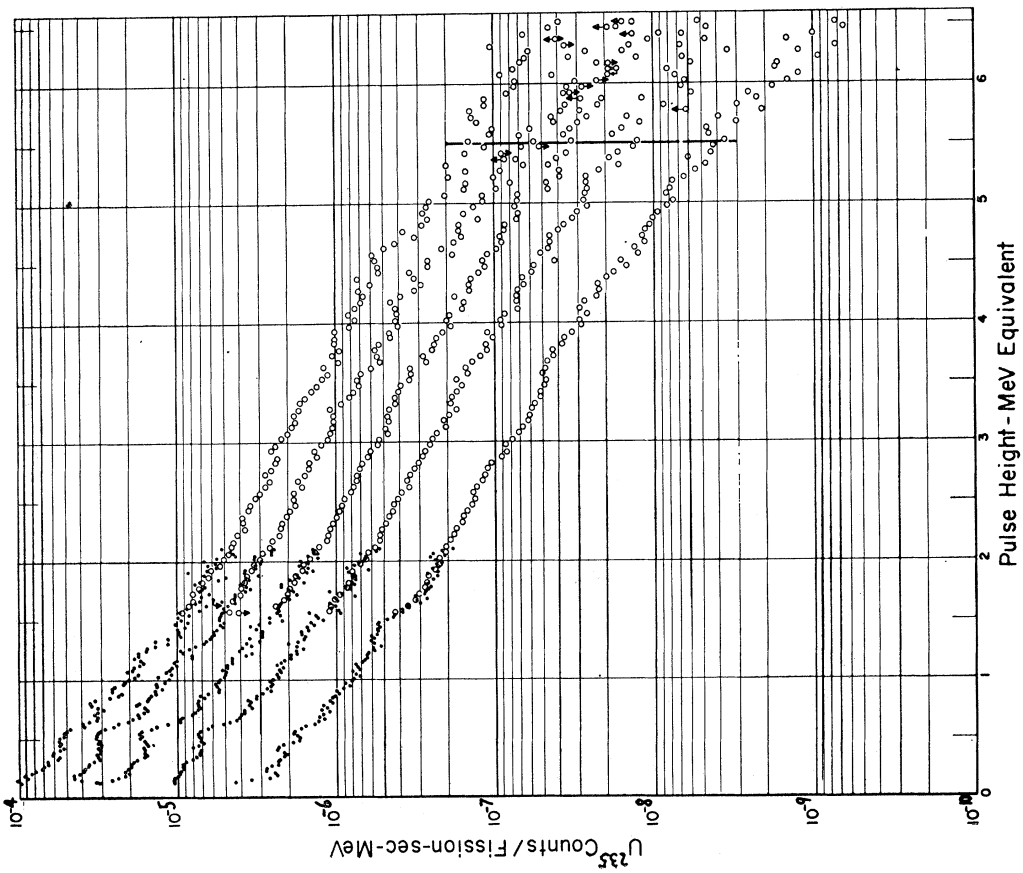

(a)

FIG. 8. Results of U^{235} differential photon spectra versus energy for different time intervals after fission expressed as (a) normalized 100-channel pulse-height distributions, and (b) fully corrected 17-bin photon distributions.

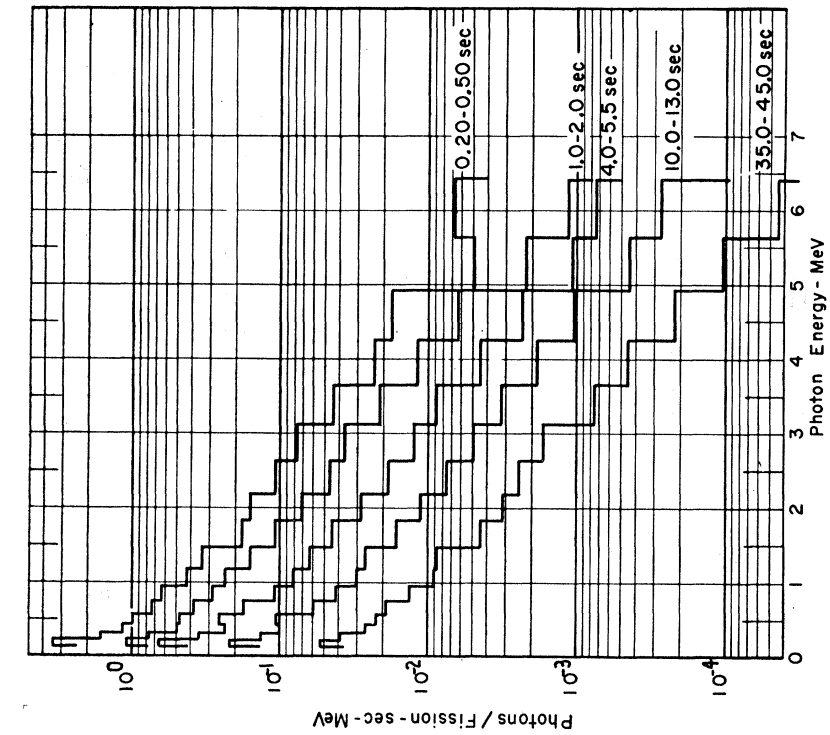

(b)

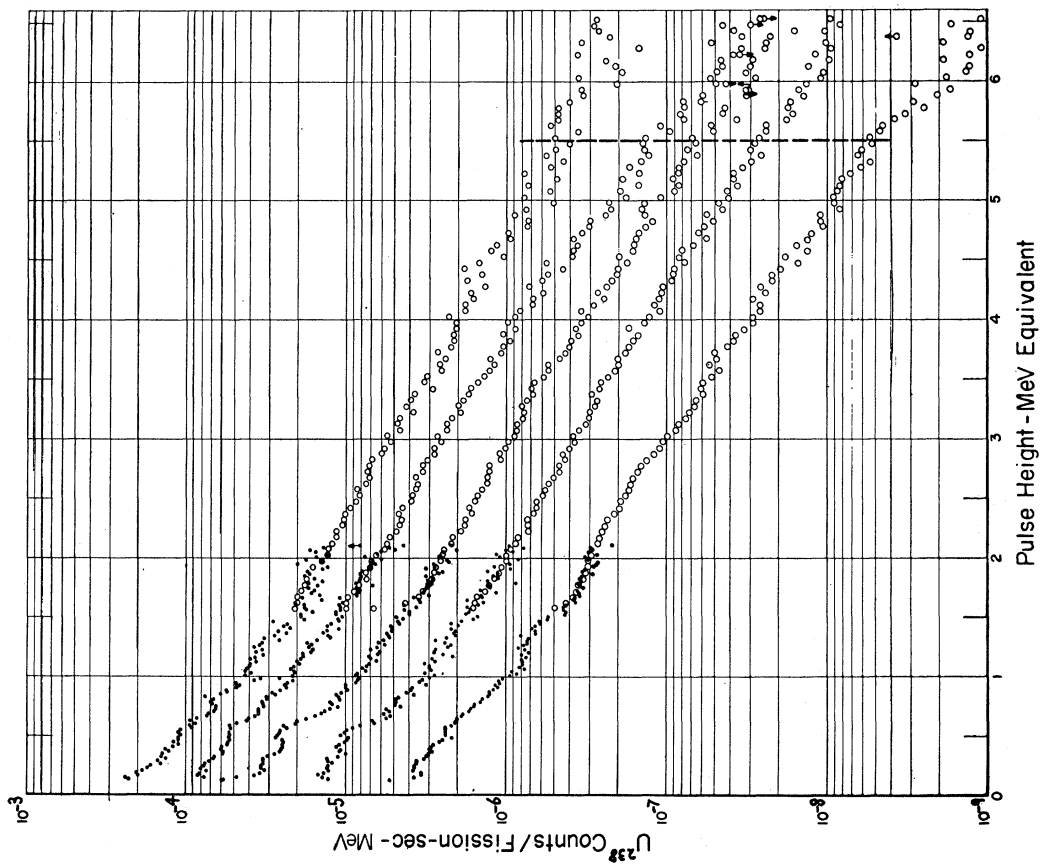

(a)

FIG. 9. Results of U^{238} differential photon spectra versus energy for different time intervals after fission expressed as (a) normalized 100-channel pulse-height distributions, and (b) fully corrected 17-bin photon distributions.

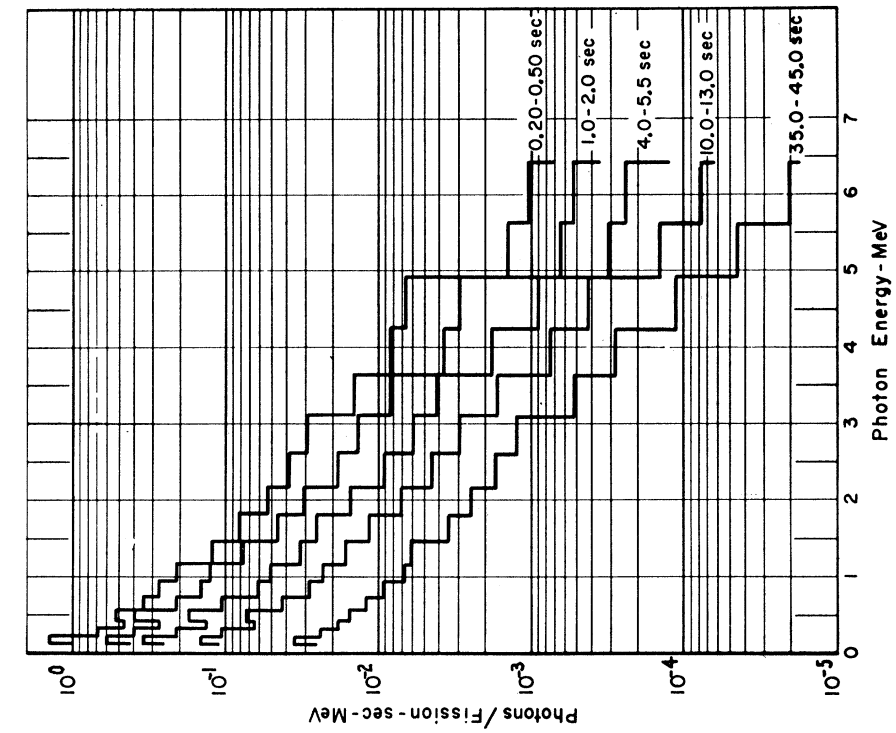

(b)

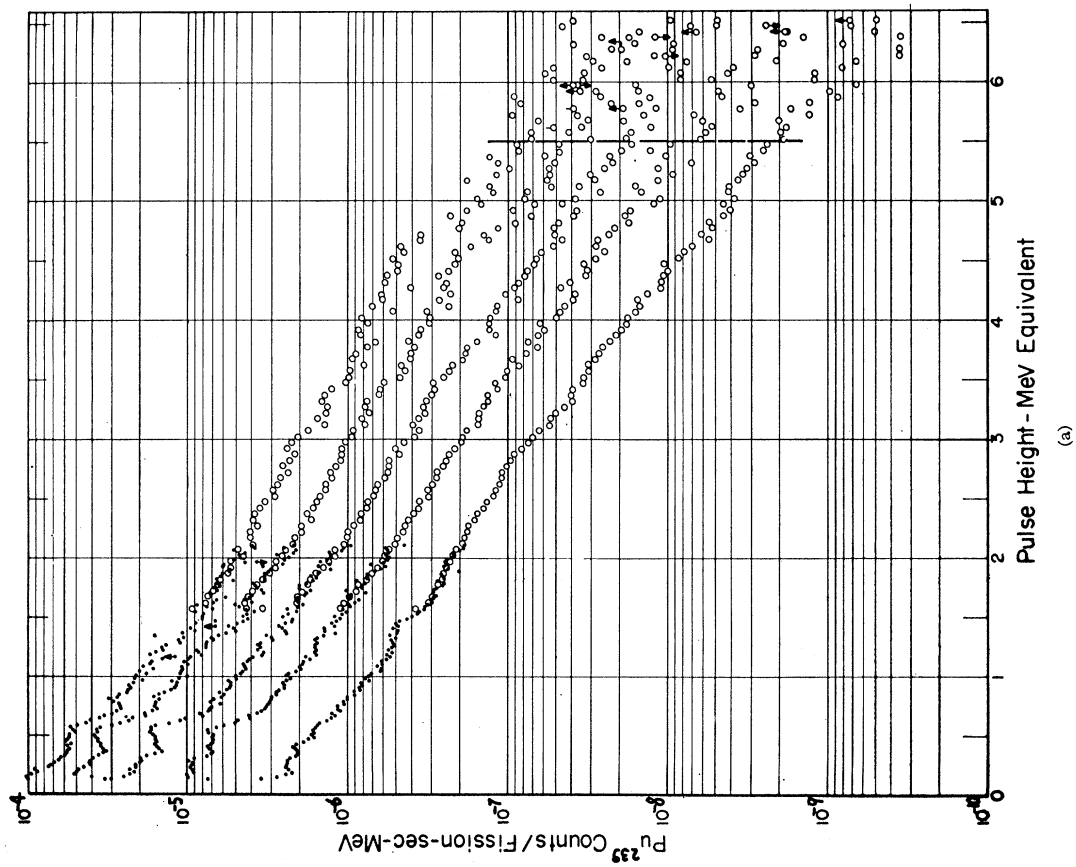

(a)

FIG. 10. Results of Pu^{239} differential photon spectra versus energy for different time intervals after fission expressed as (a) normalized 100-channel pulse-height distributions, and (b) fully corrected 17-bin photon distributions.

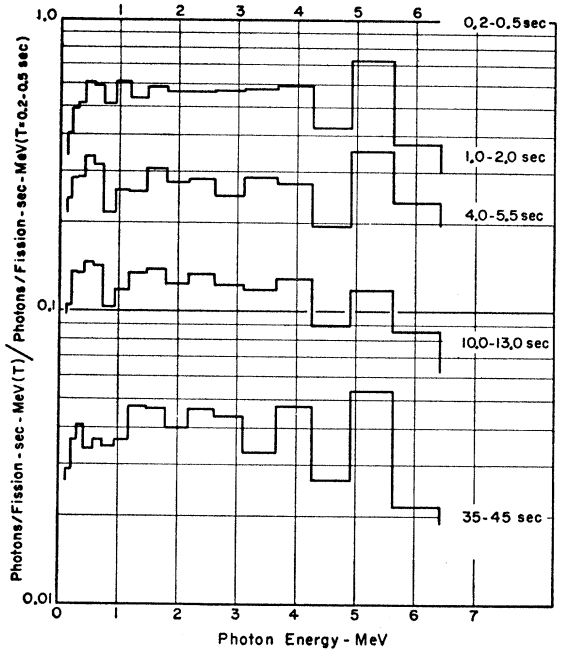

(a)

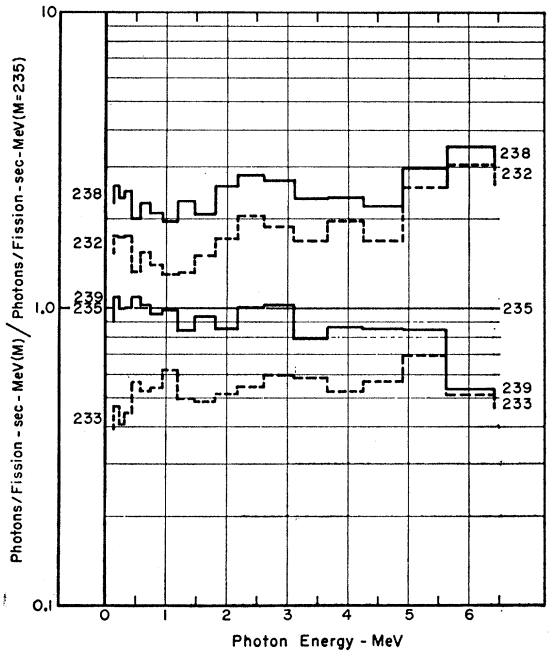

(b)

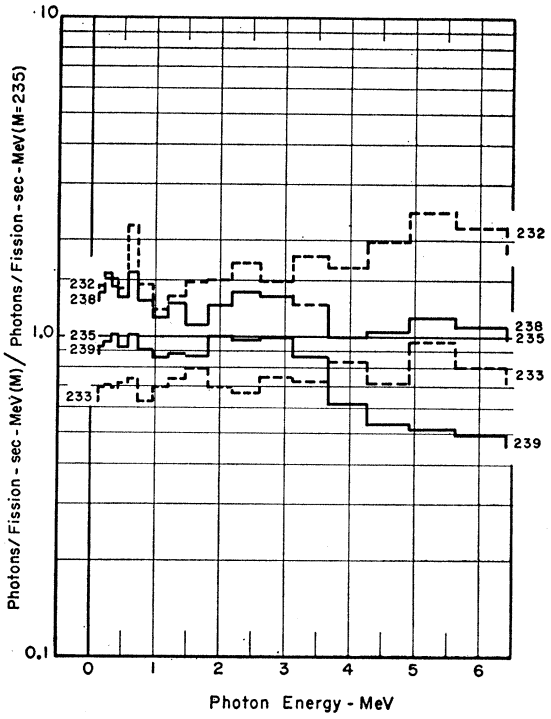

(c)

FIG. 11. (a) Ratios of 17-bin photon distributions of U^{235} normalized to unity for the 0.2–0.5 sec time interval. (b) Relative shape of different isotopes' 17-bin photon spectra versus energy, based on the U^{235} spectrum being unity for the 0.2–0.5 sec time interval after fission. (c) Relative shape of different isotopes' 17-bin photon spectra versus energy, based on the U^{235} spectrum being unity for the 35–45 sec time interval after fission.

neglected. The error components of group A are associated with both the spectrum unfolding procedure, and the experimental conditions under which pulse-height distributions were measured. A summary of the standard deviations of the various components for several representative sets of data is given in Table VI. The topmost line in Table VI presents the statistical error in the counts/bin actually measured.

Inspection of the first error listed under category A shows that the statistical error associated with the

TABLE VI. Estimated percentage errors in U^{235} and Pu^{239} photon distribution from data taken 0.2 to 0.5 sec after fission.

	U^{235}					Pu^{239}				
Bin midpoint energy (MeV)	0.175	1.075	2.405	3.956	5.277	0.175	1.075	2.405	3.956	5.277
Original statistics in counts/bin	1.9	2.0	1.3	2.2	4.6	1.6	2.2	1.5	2.7	6.2
A										
Counting statistics	3.2	3.2	3.0	5.3	11.9	2.4	3.4	3.1	6.0	12.7
Crystal response	6.2	10.4	14.3	20.0	30.0	6.0	9.9	14.8	19.1	22.8
Gain calibration[a]	0.6	2.2	3.2	5.0	18.5	0.6	2.2	2.3	4.3	20.5
Analyzer distortion[b]	2.1	0	0.5	0	0	2.3	0	0.1	0	0
Background	0.5	0.1	0.1	0.1	0.2	0.1	0.1	0.1	0.1	0.4
Sample self absorption[b]	0.5	0.1	0.1	0.1	0.1	0.7	0.1	0.2	0.2	0.2
5 MeV scale normalization	...	...	2.9	2.9	2.9	...	...	3.1	3.1	3.1
Total (rms) A	7.3	11.0	15.2	21.5	37.0	6.9	10.6	15.6	20.0	33.0
B										
Counts/fission			6.2					20.0		
Time decay normalization			3.5					3.5		
Total (rms) B			7.1					20.5		
Combined A and B (rms)	10.2	13.1	16.7	22.5	38.0	21	23	26	29	39
C										
Pulse pileup	0	0.6	13	20	37	0	0.6	8	15	28

[a] Gain error at each energy of ±1.4%.
[b] Assumed error was ±10% of correction.

calculated photons/bin for a given bin in a photon distribution is larger than the error associated with the same bin of the measured pulse-height distribution. This error amplification is inherent to the spectrum unfolding operation, and arises because the transformation is really only applicable to the results obtained from an infinite series of experiments done under identical conditions. Using barred and unbarred quantities to denote, respectively, the results from the infinite and actual finite series of experiments, the variables may be written in matrix notation as

$$\begin{aligned} &P=\bar{P}+\Delta(P)=\text{measured count distribution},\\ &\gamma=\bar{\gamma}+\Delta(\gamma)=\text{emitted photon distribution},\\ &R^{-1}=\bar{R}^{-1}+\Delta(R^{-1})=\text{inverse of crystal response}. \end{aligned} \tag{4}$$

The Δ terms represent the error in the experimentally determined variables. Combining these expressions with the matrix equations

$$\begin{aligned} &\bar{\gamma}=\bar{P}\bar{R}^{-1}\\ &\gamma=PR^{-1}, \end{aligned} \tag{5}$$

results in the following expression for the photon distribution error,

$$\Delta\gamma=\Delta PR^{-1}+P\Delta R^{-1}. \tag{6}$$

Upon simplifying the last term, and converting to numerical values, and using σ to denote the value of a standard deviation, the square of the error in the ith photon bin is found to be

$$\sigma^2(\gamma_i)=\sum\sigma^2(P_j)(R_{ij}^{-1})^2+\sum(P_jR_{ij}^{-1})^2\sigma^2(R_{ij}). \tag{7}$$

The first term in this error expression comes from the statistical error in the pulse-height distribution, while the second term is due to the inaccurate determination of the crystal's response to photons of energy i. The error given for the crystal's response is the rms sum of the crystal line shape response and the crystal absolute total efficiency.

The principal group A error due to experimental conditions arose from variations in amplifier gain which occurred during the experiment. The relatively small remaining errors arose from the correction for pulse-height analyzer distortion in low channels, the background and sample self-absorption corrections, and from inaccurate normalization of the 0.05-MeV to the 0.02-MeV resolution data.

The first of the two group B errors comes from the measurements in which the absolute number of counts in a given pulse-height interval per fission for the 10- to 13-sec time interval after fission were determined. The second group B error comes from the uncertainty in instantaneous count rate of the time decay data which were employed to obtain absolute values at times other than 10 to 13 sec after fission. Each of the samples possessed a sufficiently high concentration in the isotope whose fission products were to be observed that no correction for impurities was made.

Two conditions which might mistakenly be labeled errors have been omitted from the above discussion. One of these conditions is the time throughout which it was experimentally desirable to make a measurement. No attempt has been made to correct each photon spectrum to its appropriate value at one instant of time. The second condition arises from the rather low energy resolution inherent to the crystal response matrix. For example, the relatively low counting rate in the 100-channel distribution occurring at 0.5 MeV is transformed to a relatively high emission rate in the photon distribution.

The pulse pileup error, category C, can be obtained with the aid of the spectrum of double pulses of pulse height j, $P(\epsilon_j)$, which is given by

$$P_{\text{pileup}}(\epsilon_j)=2\tau\int_0^{\epsilon_j} P(\epsilon_i)P(\epsilon_j-\epsilon_i)d\epsilon_i. \quad (8)$$

The value of the effective pulse width τ to be used is 0.9 μsec and was obtained from measurements of the time behavior of amplifier output pulses. If two photons arrive at the crystal less than 0.9 μsec apart, an output pulse equal in height to the sum of the heights of the individual pulses will occur. Although they are often of rather noticeable size, pileup corrections to the data were not made because they normally were smaller than the combined error from matrix amplified statistics and varying amplifier gain. Calculated values of pileup in Table V for bin 14, centered at 3.96 MeV, are given to provide a convenient index to the importance of the effect in the various spectra. An experimental evaluation of pileup effects was attempted by plotting relative spectral shape as a function of counting rate, just as was done for the low-channel distortion correction described previously. The crude measured values were comparable in size to those found from the calculation procedure above.

C. Energy Integrated Spectra

Table VII gives values of photons/fission-sec which result from a straightforward integration over photon energy of the differential spectra. MeV/fission-sec were obtained by multiplying the differential spectra by the photon energy at the center of each bin and then integrating over photon energy. Values of MeV/photon in Table VII, for the different time intervals after fission, were obtained by a simple division of the two preceding quantities. Figure 12 graphically portrays the time dependence of the number of photons/fission-sec given in the table.

TABLE VII. Results of delayed gamma spectra integrated over energy for different time intervals after fission.

Isotope	Time interval (sec)	Photons/ fission-sec	MeV/ fission-sec	MeV/ photon
232	0.2– 0.5	0.966	0.916	0.948
	1.0– 2.0	0.487	0.501	1.029
	4.0– 5.5	0.267	0.246	0.921
	10.0–13.0	0.118	0.112	0.949
	35.0–45.0	0.0343	0.0343	1.000
233	0.2– 0.5	0.312	0.303	0.971
	1.0– 2.0	0.189	0.177	0.937
	4.0– 5.5	0.0958	0.0885	0.924
	10.0–13.0	0.0490	0.0465	0.949
	35.0–45.0	0.0161	0.0161	1.000
235	0.2– 0.5	0.613	0.564	0.920
	1.0– 2.0	0.324	0.311	0.960
	4.0– 5.5	0.169	0.153	0.905
	10.0–13.0	0.0775	0.0706	0.911
	35.0–45.0	0.0225	0.0221	0.982
238	0.2– 0.5	1.42	1.32	0.930
	1.0– 2.0	0.636	0.618	0.972
	4.0– 5.5	0.289	0.255	0.882
	10.0–13.0	0.110	0.0988	0.898
	34.0–45.0	0.0303	0.0281	0.927
239	0.2– 0.5	0.608	0.529	0.870
	1.0– 2.0	0.344	0.296	0.860
	4.0– 5.5	0.166	0.138	0.831
	10.0–13.0	0.0746	0.0624	0.836
	35.0–45.0	0.0209	0.0197	0.943

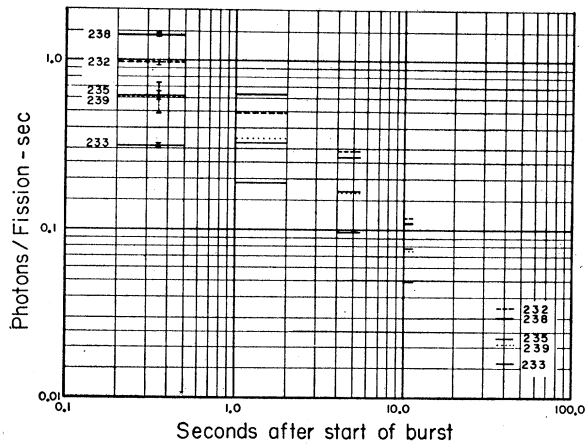

FIG. 12. Time dependence of photon emission rate derived from 17 bin photon spectra of the common fissionable isotopes. Individual spectra were integrated over energy for the different time intervals after fission.

Inspection of Tables V and VI is sufficient to indicate that for all practical purposes, a nominal error of $\pm 12\%$ should be assigned to each value of photons/fission-sec and MeV/fission-sec. For the Pu^{239} data the error in these quantities must be set at about $\pm 23\%$ because of the previously mentioned difficulty in the radiochemical determinations of absolute number of fissions in a given sample. Pileup effects are relatively unimportant because photons above about 3 MeV make an almost negligible contribution to the integrated values of Table VII. The error in all MeV/photon results is a nominal $\pm 15\%$.

D. Time and Energy Integrated Spectra

Calculated values of the total number of photons/fission, MeV/fission, and MeV/photon are given in Table VIII. The first quantity was obtained by simply fitting each set of Fig. 12 data to a five-parameter polynomial and then integrating over time from 0.2 to 45.0 sec after fission.

TABLE VIII. Results for delayed gamma spectra integrated over energy and time, from 0.20 to 45.0 sec, after fission.

Isotope	Photons/fission	MeV/fission	MeV/photon
232	5.07±0.71	5.04±0.71	0.99±0.15
233	2.02±0.28	1.97±0.28	0.98±0.15
235	3.31±0.46	3.18±0.45	0.96±0.14
238	5.50±0.77	5.08±0.71	0.92±0.14
239	3.26±0.82	2.86±0.71	0.88±0.13

The error associated with the time integration itself was determined with the aid of the time decay data mentioned in Sec. IID. Measurements of the time rate of decay of all pulses produced by photons greater than 0.1 MeV were normalized to the average of the 10–13 sec and 35–45 sec data points for each isotope of Fig. 12. The normalized time decay curve was then integrated over the 0.2- to 45.0-sec time interval. Within the statistical plus calculation error of about 5% the answer for photons/fission obtained by this method was equal to the value obtained by integrating over the polynomial previously described. Consequently the error in photons/fission is conservatively set at $\pm 15\%$ for all results except for Pu^{239} where a $\pm 25\%$ error has been assigned. For all practical purposes, the MeV/fission errors are the same as photon/fission errors.

A nominal value for the error in the MeV/photon result is $\pm 15\%$. This error arises primarily from the crystal response and gain calibration uncertainties.

V. DISCUSSION

Some comment about the experimental results given in the preceding sections and the systematic behavior indicated by them are presented here. Typical experimental errors in the absolute values of differential gamma spectra are about 10, 15, and 35% at gamma energies of 0.2, 2.4, and 5.3 MeV, respectively. Integration of these spectra over energy provided effectively instantaneous values of photons/fission-sec, MeV/fission/sec, and MeV/photon during the five different time intervals after fission. Nominal experimental errors of about $\pm 15\%$ have been assigned these integrated values. To within this error, no difference in instantaneous values of MeV/photon was measured.

However, a clear indication that different fissionable isotopes lead to inherently different energy emission rates was found. This rate can be expressed in terms of photons/fission-sec as well as MeV/fission-sec because of the essentially constant MeV/photon.

With the possible exception of the 35–45 sec time interval data, inspection of data like that shown in Fig. 11(a) reveals no particular variation with time of the hardness of a given fissionable isotope's differential spectra. The rate of emission of photons above about four MeV during the latest time interval does seem smaller than that during all earlier time intervals by a barely perceptible ($\sim 15\%$) amount. Data given in this paper are not sufficiently precise to establish the existence (or lack of existence) of a continual change in hardness of a given fissionable isotope's delayed gamma spectra. Inspection of Fig. 11(b) and (c) clearly indicates that real differences in spectral hardness do exist, and arise from the various fissionable isotopes used. The three common uranium isotopes all yield spectra of comparable hardness. By contrast the Th^{232} and Pu^{239} spectra are noticeably harder and softer, respectively, than the average uranium spectrum. While these differences appear in all five time intervals investigated, they are relatively more pronounced at later times after fission. While figures similar to the several parts of Fig. 11 and presenting data for the other time intervals and isotopes are available,[31] they contribute no more significant new information.

By concentrating attention on times in the range of one to 10^{-2} sec after fission, when few beta decays occur, Griffin[1] has quite successfully predicted the early time emission rates that were measured. His results are based on a parameter $\bar{z}$, defined as the average displacement of the initial fission fragment distribution from stability. The absolute amount of delayed gamma energy emitted (from 0.2 to 45 sec after fission) by the different fissionable isotopes can also be ordered by $\bar{z}$, although integrating the gamma emission rate over time does result in the ordering being less clear cut. Keepin's[32] attempt to correlate measured values of absolute delayed neutron yield with a parameter similar to $\bar{z}$ was still less successful. However, an approximate arrangement of isotopes by $\bar{z}$, delayed neutron yield, and delayed gamma energy emitted, can be made. The quantities for the five isotopes fall roughly into three groups, the isotopes in these groups being: 1st, Th^{232} and U^{238}, 2nd, U^{235} and possibly Pu^{239}, and 3rd, U^{233}.

As yet no detailed interpretation has been given of either the variations in spectral hardness or the variations in energy emission rate exhibited at times of the order of tens of seconds after fission. Both of these types of variation also arise from the differences in fissionable isotopes used. Further experimental insight should be provided by consideration of the more extensive time decay data available and the relatively brief results from fission of U^{234}, U^{236}, Np^{237}, and Pu^{240} mentioned in the introduction. Analysis of this type of data, for inclusion in a second paper, is now in progress.

ACKNOWLEDGMENTS

A number of people have made important contributions to the success of this experiment. Absolute photopeak efficiencies were obtained with the aid of C. H. Reed, who determined the activity of a number of our calibration samples by β-γ coincidence measurements. N. Jarmie and R. C. Allen and R. B. Day assisted in the Van de Graaff measurements of crystal response at the higher photon energies. Radiochemical determinations of absolute number of fissions for particular irradiated samples were performed under the direction of G. W. Knobeloch.

Fabrication of the disk-shaped fissionable material samples was carried out by several different groups at Los Alamos. The U^{235} and U^{238} samples were rolled and electropolished to the desired thickness under the direction of J. Anderson. The U^{233} and Pu^{239} samples were

[31] L. B. Engle and P. C. Fisher, LAMS-2642, 1962 (unpublished).

[32] G. R. Keepin, J. Nucl. Energy 7, 13 (1958).

prepared by J. Kircher and R. Tate, respectively. Mass analysis for isotopic composition of these materials was performed by L. Sturgess.

The preliminary measurements from which this experiment was designed, were performed with P. G. Koontz. A number of helpful discussions during the design stage were also had with J. D. Gallagher, J. Malik, J. D. Orndoff, H. C. Paxton, G. E. Hansen, T. F. Wimett, and G. R. Keepin. Most of these individuals also provided advice and assistance during the data acquisition and/or analysis portions of the experiment. M. P. Kellogg's assistance during both of these portions of the work is gratefully acknowledged. Several extremely helpful discussions about delayed fission gammas and NaI measurements and errors were had with H. W. Koch of the National Bureau of Standards and R. W. Peelle of the Oak Ridge National Laboratory.

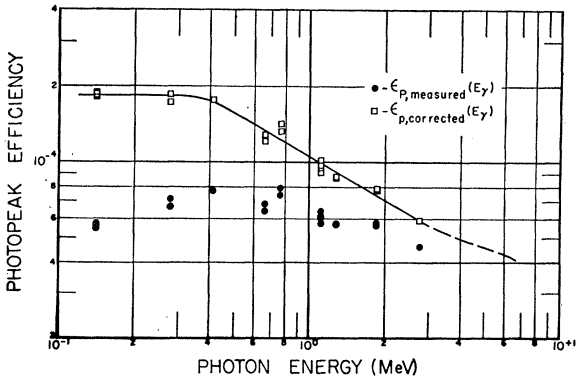

FIG. 13. Determinations of full-energy-peak efficiency $\epsilon_{p\text{measured}}(E_\gamma)$ of 4-in.-diam×4-in.-long NaI crystal in experimental arrangement of Fig. 1. Also shown are values of $\epsilon_{p\text{corrected}}(E_\gamma)$ which were obtained by the procedure described in the text.

APPENDIX: CRYSTAL CALIBRATION

A. Absolute Efficiency

1. Photopeak Efficiency

The total efficiency $\epsilon_\Sigma(E_\gamma)$ of the crystal for gammas of different energy was obtained from measurements of the absolute efficiency, $\epsilon_{p\text{ measured}}(E_\gamma)$ for detection of a given energy gamma E_γ in the full energy peak, and the ratio $f(E_\gamma)$ of counts in the full energy peak to counts in the complete pulse-height distribution. A number of simple gamma spectra from radioactive and accelerator sources were used. There was concern about the validity of using simply calculated values of efficiency for $f(E_\gamma)$ because (1) collimator edge penetration effects were known to be of noticeable size; (2) the precise influence of the thick CH_2 β-absorber on gamma line shape was difficult to predict; (3) the crystal was oriented in such a way that gammas were incident on the curved surface. Consequently an empirical approach was adopted.

The actual experimental geometry was calibrated using a "standard" NaI crystal of known photopeak efficiency, $\epsilon_{pst}(E_\gamma)$, to evaluate $\epsilon_{p\text{ measured}}(E_\gamma)$. The standard was a $1\frac{1}{2}$-in.-diam×$1\frac{1}{2}$-in.-long NaI crystal rigidly mounted on a 6292 photomultiplier. Samples on $\frac{3}{4}$-in.-diam filter paper disks were precisely positioned about $\frac{1}{2}$ in. from, and coaxial with, the crystal. Original calibration was made with samples whose activity had been determined by β-γ coincidence techniques; in some cases the activity of the solution from which such a sample came had been checked by $4\pi\beta$ counting. From these sources of known strength, the full energy peak efficiency for a given E_γ was found. Deviation of any measured $\epsilon_{pst}(E_\gamma)$ point $\geq$0.412 MeV from a straight line least-squares fit was never larger than 2.4%. It is believed that the smooth curve drawn through the points having E_γ less than 0.412 MeV fixed $\epsilon_{pst}(E_\gamma)$ within about 2%.

To minimize geometry effects, only the full energy peak of a gamma pulse-height distribution was used for the large crystal efficiency determinations. The main difficulties encountered in calibrating this crystal were in obtaining high-activity samples of large enough mass to be accurately weighed and yet small enough size to fit into the fissionable material sample volume allowed by the transfer tube. Sum line corrections[33] were always less than 1%. A set of samples of a given isotope usually consisted of two samples for use with the large crystal geometry, and two sets of dilute solutions from each of which at least three specimens were made for comparison with the standard crystal. The ratio of the activity in the large crystal sample to the activity in the standard crystal specimen varied from 5×10^2 to 5×10^3. Sample size was determined by weighing the bulk materials or 50λ aliquots of the different solutions employed. Radiochemical purity of half of the source materials was tested by measuring the full energy peak counting rate and $f(E_\gamma)$ at times at least two months or one half-life apart. For the sources checked, only negligible amounts ($\lesssim$2%) of activities having periods much shorter than the inspection time interval could have been present. The measured values of full-energy-peak efficiency are given in Fig. 13.

It was assumed that the two stage calculation described next would yield the most accurate value of photopeak efficiency $\epsilon_p(E_\gamma)$. The values of $\epsilon_{p\text{ measured}}(E_\gamma)$ were corrected for absorption effects in the CH_2 filter and in the wall of the source holder. Then a collimator edge penetration correction was applied at each E_γ to reduce all effective apertures to a common geometric aperture. By restricting concern to photopeak instead of total efficiency, the edge penetration calculation was easily accomplished. The fractional increase I of the solid angle due to this penetration is given by

$$I=\frac{1}{2\Omega_0}\int_{\theta_1}^{\theta_2} e^{-\mu x}\sin\theta d\theta,$$

[33] P. R. Bell, *β- and γ-Ray Spectroscopy*, edited by K. Seigbahn (North-Holland Publishing Company, Amsterdam, 1955), p. 157.

where Ω_0 is the geometric aperture, μ is the total absorption coefficient excluding coherent scattering (see Grodstein[34]) of the collimator material, and x is the path length in the collimator of a gamma emitted from the source inclined at an angle θ with respect to the center line through the source and collimator.

From all of the above a set of points $[\ln\epsilon_{p\text{ corrected}}(E_\gamma), \ln E_\gamma]$ was derived. A straight line was least-squares fitted to the measurements of $E_\gamma \geq 0.412$ MeV on the assumption that the two variables in the set were linearly related. Within 0.5% in efficiency, the same straight line was obtained if the 0.412-MeV point was omitted. A smooth curve was then drawn in to connect the medium energy least squares fit with the straight line portion in the low-energy region of Fig. 13. Upon applying the effects of edge penetration and the actual absorber used, CH_2 plus Fe carrier wall, in reverse to this curve, the variation of $\epsilon_p(E_\gamma)$ below three MeV was finally obtained.

2. *Photofraction*

Some values of $f(E_\gamma)$ shown in Fig. 14 were obtained from simple measurements of radioactive source spectra. The remaining $f(E_\gamma)$ were evaluated by an iterative procedure, working progressively toward higher E_γ. Iteration was necessary as all gammas greater than one MeV appeared in spectra which had several components. Thus, for example, Au^{198}, Cs^{137}, and Nb^{95} helped fix $f(E_\gamma)$ at 0.511 MeV. This result when combined with the photopeak counting rate of the 0.511-MeV impurity in the Zn^{65} spectrum allowed evaluation of $f(E_\gamma)$ for the 1.14-MeV Zn^{65} gamma.

Values of $f(E_\gamma)$ above about three MeV might be somewhat high because of exclusion of the effects of the 0.511-MeV gammas produced by pair production of source gammas in the Pb wall of the collimator. Some measurements of this 0.511-MeV component were made, however, positron emission tended to confuse the Y^{88} result, while internal pair formation confused the Na^{24} and the $N^{15}(p,\alpha\gamma)$ results. The measurements did indicate that the $f(E_\gamma)$ values of Fig. 14 might be too large by as much as 5% at 6.5 MeV. Below 4 MeV, a conservative estimate places the error in $f(E_\gamma)$ at about $\pm 3\%$. To obtain calibration gammas with energies greater than 2.76 MeV, the essential parts of the counting geometry were moved so that the target of a Van de Graaff accelerator could be placed at the fission sample position.

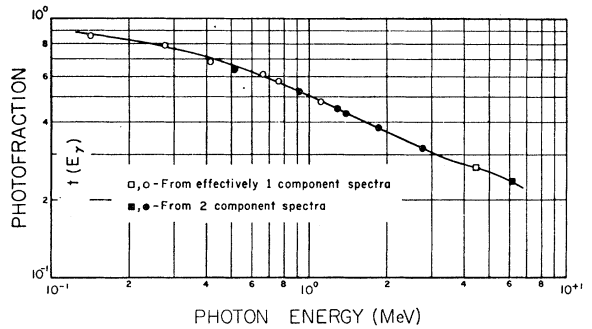

FIG. 14. Measured values of the ratio of full energy peak area to total area $f(E_\gamma)$. The circles represent data taken for the geometry shown by Fig. 1. The squares are for data taken in the geometry employing the Van de Graaff accelerator.

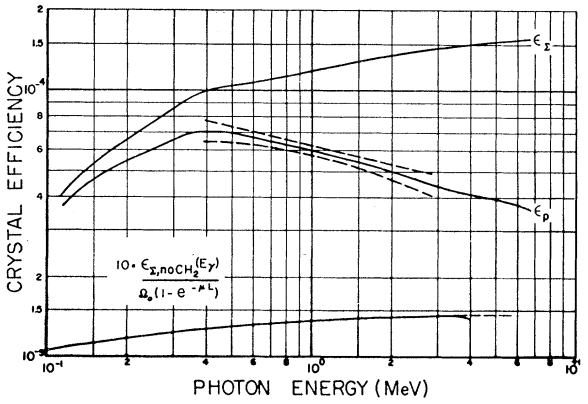

FIG. 15. Smoothed variations of $\epsilon_p(E_\gamma)$ and $\epsilon_\Sigma(E_\gamma)$ found from results of Figs. 13 and 14. Variation of the total efficiency in a geometry lacking a polythene absorber, normalized by multiplying by 10^{-5} to obtain a suitable ordinate, is also shown.

3. *Total Efficiency*

Division of $\epsilon_p(E_\gamma)$ by $f(E_\gamma)$ yielded the desired total detection efficiency $\epsilon_\Sigma(E_\gamma)$ given in Fig. 15 for $E_\gamma \leq 3$ MeV. The figure also gives efficiency values for higher energy gammas. The total crystal efficiency was obtained from the expression $\Omega_0(1-e^{-\mu L})$, where μ is the NaI absorption coefficient without coherent scattering,[33] and L is the average crystal thickness for gammas emitted from the source at different angles. It was then assumed that this efficiency should be equal to, or at least show a variation with energy similar to, the total efficiency calculated from the quantity $[\epsilon_{p\text{ corrected}}(E_\gamma)\cdot I$ due to edge penetration$]/f(E_\gamma)$. This ratio multiplied by 10^{-5} to normalize to the scale of Fig. 15, is shown at the bottom of Fig. 15.

Because of collimator effects which tend to give smaller $f(E_\gamma)$, and to edge penetration, the experimentally derived total efficiency is larger than the simple $\Omega_0(1-e^{-\mu L})$ prediction. Preliminary values of this ratio in the 3- to 4-MeV region were obtained by an extrapolation of the straight line least-squares fit of $\ln\epsilon_{p\text{ corrected}}(E_\gamma)$. Because the pair production cross section for Pb increases by only a factor of two in going from 3 to 6.5 MeV, and because the 0.5-MeV gammas from pair production in the Pb collimator wall appear to be a relatively small effect for $f(E_\gamma)$, it seemed reasonable to extrapolate the ratio of total efficiency

[34] G. W. Grodstein, Natl. Bur. Std. Circular #583, 1957 (unpublished).

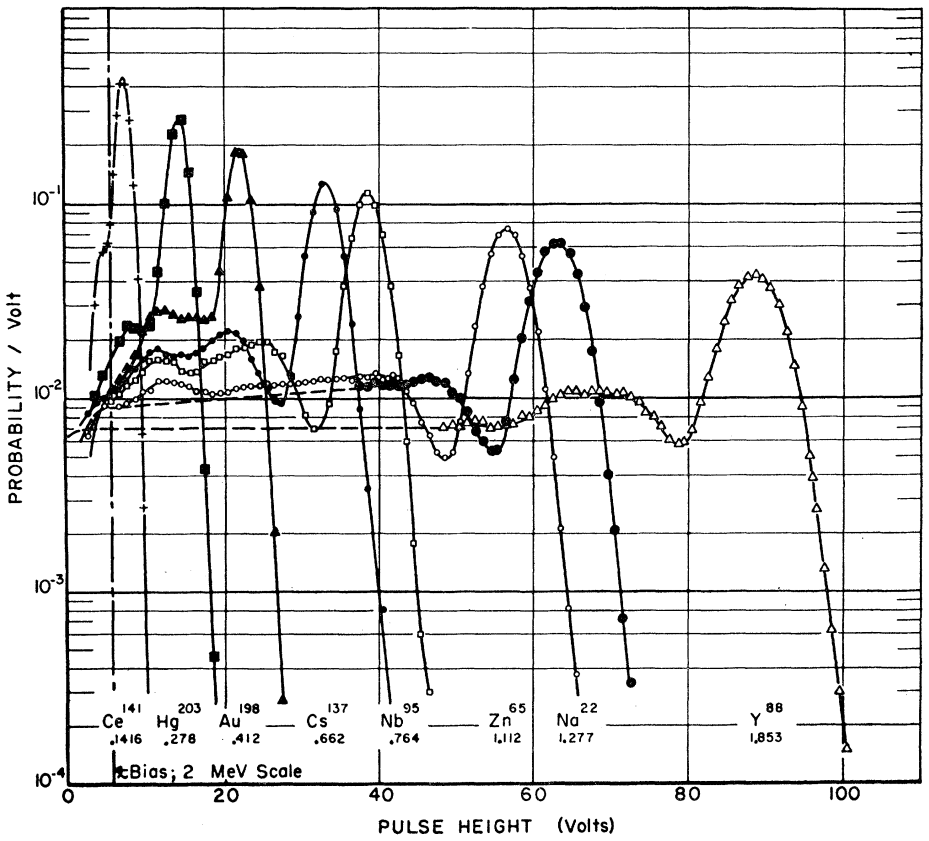

FIG. 16. Crystal response on 2-MeV scale to monochromatic incident gammas. Each curve has unit area.

along the dashed line shown in Fig. 15. As a large change in these effects seems unlikely, it is believed that the error at 6.5 MeV from using the dashed line for the total efficiency ratio should be only $\pm 5\%$ larger than the error at 3 MeV. Actually there is a little additional qualitative evidence that there is not a large error involved in using this procedure. Monte Carlo calculations[35,36] for a somewhat different geometry indicate a gentle rise near 4 MeV in both $f(E_\gamma)$ and a quantity equivalent to $\epsilon_{p\ \text{corrected}}(E_\gamma)$.

It is believed that the final values of $\epsilon_p(E_\gamma)$ and $\epsilon_\Sigma(E_\gamma)$ are known to within standard deviations of $\pm 3\%$ and $\pm 4\%$, respectively, from 0.14 MeV up to about 2.5 MeV. The dashed curves on Fig. 15, presenting the $\epsilon_p(E_\gamma)$ error's variation from a minimum of 4% to a maximum of 9%, are for an error of *two* standard deviations. Above 2.5 MeV, a crude equivalent of one standard deviation for $\epsilon_\Sigma(E_\gamma)$ might increase linearly with energy, reaching something like $\pm 9\%$ at 6.5 MeV.

A Zn^{65} and a Cs^{137} source, which were monitored throughout the experiment, indicated that no change in system full energy efficiency, within $\pm 1.5\%$, or in resolution, within an error of several percent, had occurred.

[35] W. F. Miller, J. Reynolds, and W. T. Snow, Rev. Sci. Instr. **28**, 719 (1957).
[36] M. J. Berger and J. Doggett, Rev. Sci. Instr. **27**, 269 (1956).

B. Line Shape Response

In addition to $\epsilon_\Sigma(E_\gamma)$ it was necessary to determine the pulse-height distributions which would be produced by different energy monochromatic gamma beams striking the crystal. Figures 16 and 17 give corrected line shapes and energies in MeV of the various gammas investigated, together with the activity or charged particle reaction from which the gamma appeared. Some of the curves, such as the 1.277-MeV gamma from Na^{22}, were obtained by subtracting off the contribution of a different energy gamma which also appeared in the experimental spectrum. From a knowledge of $f(E_\gamma)$ as given in Fig. 14, and the unperturbed higher energy gamma portion of the distribution which occurrs in a two gamma component spectrum, the absolute probability of detection in a given voltage interval can be found. Although the shape of that portion of the distribution mixed with the lower energy gamma must be estimated, at least the total contribution of that portion is known. Experience with one component distributions for this geometry plus comparisons with other measurements and calculations[37,38] lead to the evaluations of the

[37] R. L. Heath, *Scintillation Spectrometry Gamma Ray Spectrum Catalogue, IDO-16408* (Phillips Petroleum Company, Idaho Falls, Idaho, 1958).
[38] M. J. Berger and J. Doggett, J. Res. Natl. Bur. Std. **56**, 355 (1956).

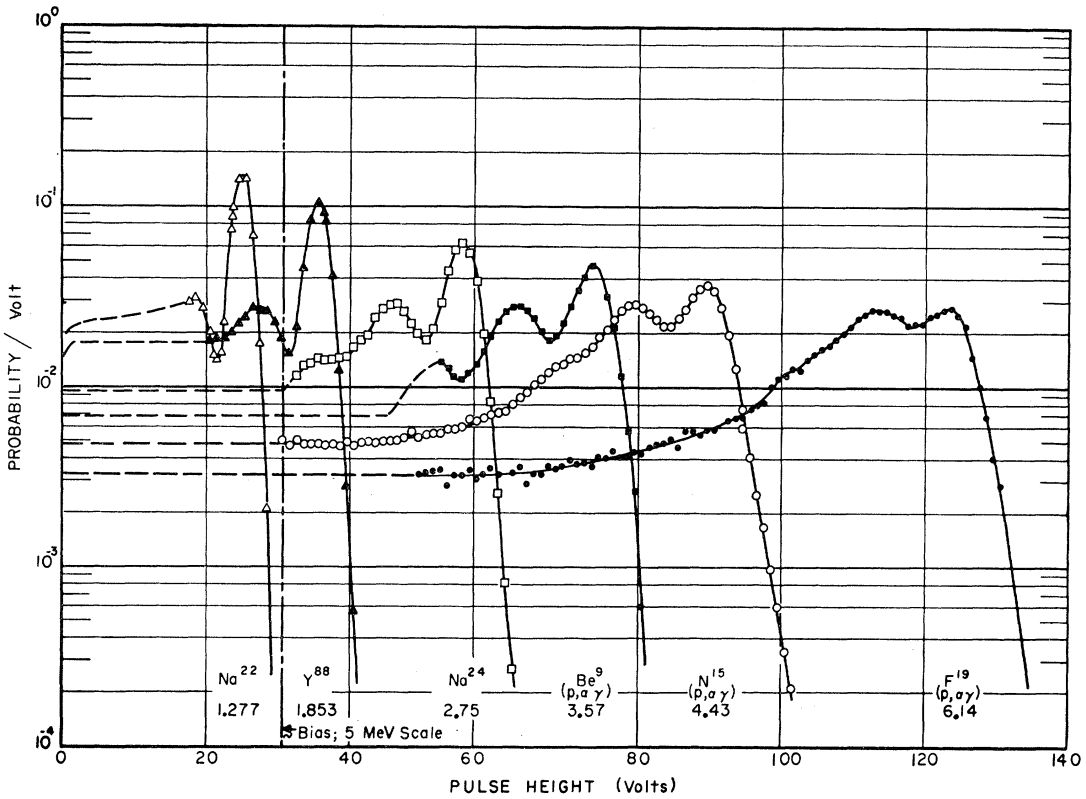

FIG. 17. Crystal response on 5-MeV scale to monochromatic incident gammas. Each curve has unit area.

unmeasured portions given by the dotted lines in Figs. 16 and 17. For the 6.14-MeV gamma from $F^{19}(p,\alpha,\gamma)$, the $\sim 13\%$ contribution of higher energy gammas was subtracted using a line shape guessed at from a knowledge of the behavior near 6 MeV. Because of the need for this subtraction, care was taken to use a suitably thin target and so produce only gammas from the resonance at 1.381-MeV proton energy.[39] The area under each distribution includes back scattered gamma effects and contributions down to 0 V, and has been normalized to unity. Below about 60 keV, the crystal container's absorption becomes increasingly severe as the line shapes on the 2-MeV scale indicate. On the 5-MeV scale, the hard to measure (because of background) low-energy tail regions of a given gamma distribution were assumed to have a constant probability of detection per volt.

[39] C. Y. Chao, A. V. Tollestrup, W. A. Fowler, and C. C. Lauritsen, Phys. Rev. **79**, 108 (1950).